Nonclogging Resistive Pulse Sensing with Electrohydrodynamic Cone-Jet Bridges

Yuejun Zhao, David B. Bober, and Chuan-Hua Chen*

Department of Mechanical Engineering and Materials Science, Duke University, Durham, North Carolina 27708, USA

(Received 9 November 2010; published 7 November 2011)

A new paradigm of resistive pulse sensing (Coulter counting) is developed using a liquid bridge in lieu of a solid pore as the sensing aperture, whereby the flexible liquid aperture circumvents the clogging issue of conventional Coulter counters. The electrohydrodynamic bridge is formed between two opposing Taylor cones and stabilized by radial polarization stresses. Passage of a colloidal particle through the upstream conical apex triggers a current oscillation at the resonant frequency of the cone-jet bridge. The relative current change is indicative of the particle-to-jet diameter ratio.

DOI: 10.1103/PhysRevX.1.021007 Subject Areas: Fluid Dynamics, Interdisciplinary Physics, Soft Matter

I. INTRODUCTION

The resistive pulse sensing technique detects and characterizes particles by the modulation of electrical current through a fluidic aperture [1]. The key component in implementing this Coulter principle is the sensing aperture which dictates the analysis range. Miniaturized pores are needed to measure small synthetic and biological entities such as quantum dots and viruses. However, microscale solid pores are expensive to fabricate and prone to clogging because of impurities and agglomerates in the sample, limiting the smallest diameter of commercial Coulter apertures to 20 μm or so [2]. Here, we address this dilemma by using a liquid sensing aperture in lieu of a solid-state one.

Adapting the well-known Taylor cone-jet [3–5], we formed a liquid-bridge sensing aperture between two opposing Taylor cones (Fig. 1). The cone-jet bridge configuration in Fig. 1 resembles the liquid bridges previously reported (e.g., [6–9]), but our case is different, with two opposing Taylor cones (unlike [6,8]) bridged by a slender jet (unlike [7,9]). In contrast to the conventional Taylor cone-jet in which surface convection current is important [5], we will show that the electrical current through the cone-jet bridge is primarily carried by bulk Ohmic conduction.

Building upon a previous proof of concept [10], we report in this paper the fundamental mechanisms of the cone-jet bridge and its application in resistive pulse sensing as a miniaturized, yet nonclogging aperture.

II. EXPERIMENTAL SETUP

The experimental setup to produce the cone-jet bridge is schematically shown in Fig. 1. The working fluid was ethylene glycol unless otherwise specified and was doped by a salt to an appropriate conductivity (measured with an Oakton 510 meter). The dopant was either potassium chloride or sodium borate, without appreciable difference in the results. The fluid was supplied by a Legato 180 syringe pump to a New Objective PicoTip nozzle with an inner diameter of 100 μm and an outer diameter of 150 μm. Through a metallic union, the working fluid was electrified between the glass nozzle and a planar counter electrode using a Trek 610E high-voltage amplifier. The counter electrode was made of black silicon [11] to ensure even spreading of the working fluid. Fluid accumulation was further prevented by gravity, which was downward and parallel to the silicon substrate. Our setup differed from typical electrohydrodynamic systems in its close nozzle-to-plate separation, usually within 0.25 mm. The close separation was crucial in enabling the cone-jet bridge.

Unlike the conventional cone-jet, *the length of the nozzle plays a role in the cone-jet bridge formation* because the bridging jet has a much larger diameter and carries a much larger current. A significant voltage drop can take place on a long nozzle, which provides an extra feedback mechanism in the electromechanical oscillation. Unless otherwise specified, short nozzles of 3 mm length were used. The short nozzle was affixed to a tubing sleeve for hydraulic

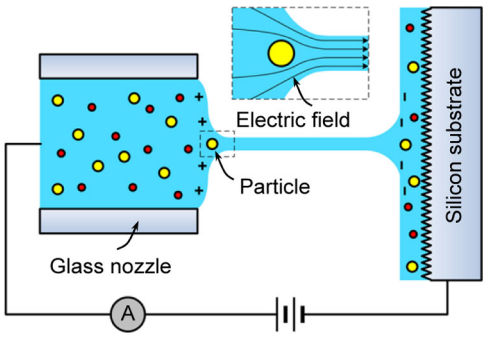

FIG. 1. Schematic of a resistive pulse sensing system in which particles are detected by the modulation of electrical current through a cone-jet bridge, a flexible sensing aperture that is not clogged by impurities.

*chuanhua.chen@duke.edu

connection. Long nozzles (20 mm) were used to promote the underdamped oscillations seen in Figs. 3–5, in part by increasing the RC time constant. A long nozzle was also used for the work described in our earlier paper [10].

The current was monitored by the voltage drop across the standard 1 MΩ resistance of an Agilent DS05014A oscilloscope. Electrical noise was minimized with a Faraday cage. The electrohydrodynamic process was visualized by a Phantom v7.3 or v710 camera through an Infinity K2 microscope. Illumination was provided by a Fiber-Lite LMI-8000 LED light source to minimize heating.

III. CONE-JET BRIDGE

We first discuss the physics of the cone-jet bridge as schematically shown in Fig. 1, including its formation, stabilization, and resonance. Our cone-jet bridge will be compared to the well-studied Taylor cone-jets [5] and electrohydrodynamic liquid bridges [12].

A. Formation

A typical formation process of the cone-jet bridge is shown in Fig. 2 (see also Video 1 [13]), which can be divided into three stages: (i) The first Taylor cone formed on the electrified nozzle out of which a conventional cone-jet emitted, leading to accumulation of the working fluid on the counter electrode; (ii) A second Taylor cone developed from the liquid accumulated on the counter electrode, and the two cones eventually merged given sufficiently close nozzle-to-plate spacing; (iii) The resulting liquid bridge between the two cones went through a series of complex morphological transitions, ultimately arriving at a stable jet bridging the two receded Taylor cones.

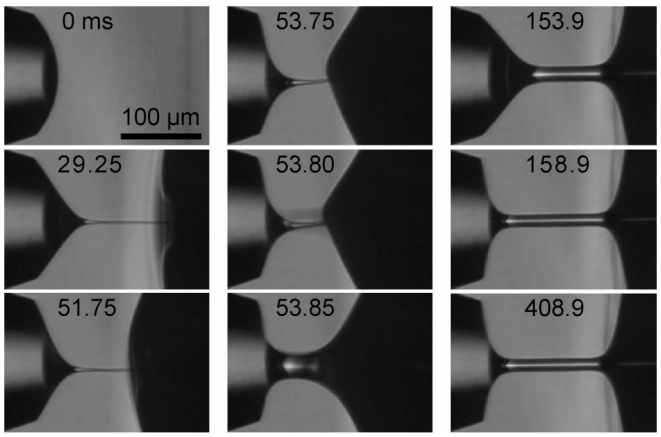

FIG. 2. The formation process of a steady cone-jet bridge. Ethylene glycol (10 μS/cm) was supplied at a flow rate of 0.20 mL/h, and electrified between the nozzle (grounded) and the counter electrode ($-$ 1.4 kV) with a separation of 0.21 mm. The diameter of the jet bridging the two cones (right column) is typically an order of magnitude higher than that of the conventional jet issued from a single Taylor cone (left column). These snapshots were captured from Video 1 [13].

The cone-jet bridge was very robust. Although the transient processes could be different from case to case, the end cone-jet bridge (shown at 158.9 ms and 408.9 ms) was almost always the same. After the system reached its steady state, even if all of the exposed liquid was blown dry, the same configuration of cone-jet bridge would typically emerge within 1 s.

Many working fluids conducive to conventional cone-jets also support cone-jet bridges (Table I), an example being the methanol-water mixture widely used in electrospray ionization. Unlike conventional cone-jets, in which a significant portion of the jet current is carried through surface-charge convection instead of bulk Ohmic conduction [17,18], the electric current through the cone-jet bridge was predominantly Ohmic. With otherwise the same condition, ethylene glycol at a higher conductivity resulted in a proportionally higher current carried by a jet of comparable diameter (Table I).

B. Stabilization

The stabilization of the cone-jet bridge is fundamentally different from the conventional Taylor cone-jet [19]. In the conventional cone-jet (Fig. 2, left column), the jet experiences a significant acceleration because of the tangential electric stresses associated with surface charges, which exert an *axial* force competing with surface tension to stabilize the jet. (The Columbic self-repulsion of the surface charges can be either stabilizing or destabilizing [20].) In the cone-jet bridge (Fig. 2, right column), the jet has a uniform diameter in the streamwise direction, indicating negligible surface charges. The absence of any appreciable surface charges is also corroborated by the merging of the two oppositely charged Taylor cones prior to the formation of the cone-jet bridge (Fig. 2, middle column). Without surface charges, the current-carrying jet is stabilized by a *radial* polarization force (see Fig. 1 of Ref. [21]). The stabilizing role of the polarization force has long been recognized, particularly in the liquid bridge literature; see, for example, Refs. [6,22–25].

In order to outcompete surface tension, the polarization stresses should satisfy

$$\frac{\varepsilon - \varepsilon_0}{2} E^2 \gtrsim \frac{2\gamma}{d_j}, \tag{1}$$

where ε and ε_0 are the permittivities of the liquid jet and the surrounding air, E is the axial electric field, γ is the surface tension, and d_j is the diameter of the jet. According to Eq. (1), the threshold electric field needed to form a stable cone-jet bridge is $E_{\text{th}} = 2\sqrt{\gamma/d_j(\varepsilon - \varepsilon_0)}$. The average electric field was estimated in two ways: $\bar{E}_I = I/(\frac{\pi}{4}\sigma d_j^2)$ was based on the assumption that the current through the jet was entirely and uniformly Ohmic;

TABLE I. Selected experimental conditions for stable cone-jet bridges compared to the theoretical stability threshold (E_{th}).

Working fluid[a]	σ (μS/cm)	V (kV)	Q (mL/h)	I (μA)	d_j (μm)	$\bar{E}_I$ (kV/mm)	$\bar{E}_V$ (kV/mm)	E_{th} (kV/mm)
Ethylene glycol[b]	3.0	1.45	0.20	0.4	16	6.9	5.8	6.1
Ethylene glycol	10.0	1.45	0.20	1.2	15	7.0	5.8	6.3
Methanol-water[c]	5.0	1.38	0.50	0.5	19	3.8	5.5	3.9

[a]With a given working fluid and given conductivity (σ), a voltage (V) was applied with a fixed nozzle-to-plate separation (L) of 0.25 mm. The flow rate (Q) was slightly above the minimum necessary to generate a stable cone-jet bridge, for which a very limited range of voltages could stabilize the system; within this range, a medium voltage was selected. The current (I) was measured together with the approximately uniform diameter (d_j) of the jet.
[b]Ethylene glycol was doped to a conductivity of 3 μS/cm or 10 μS/cm. Except for the measured conductivity, other properties were assumed the same as those of the pure liquid [14].
[c]Methanol:water mixture was 1:1 by volume and doped to 5 μS/cm. Other properties of the mixture were taken from the literature [15,16].

$\bar{E}_V = V/L$ was a nominal field equal to the applied voltage divided by the nozzle-to-plate separation. As shown in Table I , the estimates for the applied fields ($\bar{E}_I$ and $\bar{E}_V$) are consistent with each other, and are around the scaling threshold for different working fluids (E_{th}).

The scaling analysis in Eq. (1) explains why the cone-jet bridge has not been reported in conventional cone-jet systems, where the nominal field is typically on the order of 0.1 kV/mm and the liquid jet is typically micrometric ([5] and references therein). Under such conditions, the polarization pressure is insufficient to overwhelm the capillary pressure. On the other hand, pinned liquid bridges have been stabilized at fields comparable to 0.1 kV/mm, although these liquid cylinders are typically millimetric, and the capillary pressure is therefore much lower ([12] and references therein).

C. Resonance

The cone-jet bridge exhibits a clear resonance in its electromechanical oscillations. In a typical oscillation of the cone-jet bridge, particularly around the resonant frequency, the jet diameter oscillates uniformly along the entire length of the bridging jet (Fig. 3; see also Video 2 [26]). This peculiar oscillation mode is a consequence of the balance between the stabilizing polarization force and the destabilizing capillary force, and, in turn, the suppression of the varicose instability.

To first order, the cone-jet bridge can be modeled as two conical oscillators in series with a bridging-jet oscillator. The resonant frequency of the cone scales as the Rayleigh frequency of a spherical drop of comparable size [15,27,28],

$$f \sim \sqrt{\frac{\gamma}{\rho d_n^3}}, \tag{2}$$

where ρ is the liquid density and d_n is the *wetted* diameter of the nozzle on which the cone is attached. Since the capillary frequency is much higher for the jet ($d_j \ll d_n$), the resonant frequency of the cone-jet bridge is governed by the conical oscillation (which is the softer "spring"). For 150 μm nozzles, the measured resonant frequency (Fig. 4) was about half of the capillary frequency in Eq. (2). The qualitative trend of decreasing resonant frequency with increasing diameter, predicted by Eq. (2), was confirmed using glass nozzles of different outer diameters (30, 150, and 330 μm). However, we were not able to conclusively verify the $d_n^{-3/2}$ power law because of the following constraints: The voltage-flow rate ($V - Q$) operating diagram of the cone-jet bridge was very sensitive to the nozzle diameter (d_n); therefore, it was difficult to maintain the same V and Q for different d_n. Maintaining a uniform conical shape across different nozzle diameters also proved to be challenging.

The cone-jet bridge is a unique electrohydrodynamic system: (i) Unlike a conventional cone-jet whose configuration is not a function of the downstream condition on the counter electrode [21,29], the cone-jet bridge was formed by an inverse cone issued from the counter electrode and was therefore a strong function of the downstream condition (e.g., fluid accumulation as shown in Fig. 2).

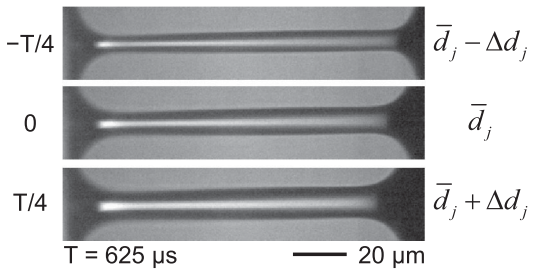

FIG. 3. The forced oscillation of the cone-jet bridge, in which the average diameter along the jet (d_j) fluctuates with a period (T). The oscillation was driven by a sinusoidal voltage at 1.6 kHz with a peak-to-peak amplitude of 20 V, superimposed on the base voltage of 2.4 kV. The flow rate of ethylene glycol (5.2 μS/cm) was 0.2 mL/h, and the nozzle-to-plate separation was 0.2 mm. A long nozzle (20 mm) was used to promote oscillations, as discussed in Sec. II. These snapshots, spanning half a period, were captured from the top half of Video 2 [26].

(ii) Unlike a conventional liquid bridge whose ends are pinned [6,23], our bridging jet was connected to the Taylor cones at both ends and therefore cannot be treated as an isolated bridge. The resonant oscillations discussed above clearly demonstrated these differences by the concerted dynamics of the entire cone-jet bridge (Fig. 3). The resonance of the cone-jet bridge and its Ohmic nature are essential to the interpretation of the resistive sensing results in the next section.

IV. RESISTIVE PULSE SENSING

We will now describe the use of the Ohmic cone-jet bridge for resistive pulse sensing of colloidal particles. A particle passing through the conical apex triggers an oscillation of the bridge, and the resulting current change is indicative of the particle volume.

A. Particle-triggered oscillation

When a particle passes through the cone-jet bridge, it triggers modulations of both electric current and mass flow (Fig. 5). The particle-triggered oscillation was at the resonant frequency of the cone-jet bridge (Fig. 4). Within a very small uncertainty ($\pm$ 20 μs in Fig. 5; see also Video 3 [30]), the first minimum jet diameter always synchronized with the presence of the particle at the apex of the upstream cone. This synchronization was observed regardless of the particle size, the nozzle length, and the imposed flow rate (which partially controlled the convective velocity of the particle).

The synchronization motivates the following scaling arguments for the oscillation amplitude. For the cone-jet bridge of ethylene glycol, the flow through the upstream cone due to the imposed flow rate $\bar{Q}$ is dominated by an ideal sink flow [17,31]. When a particle of diameter d_p and volume V_p reaches the tip of the conical apex, the fluctuation conceivably reaches a maximum. Owing to the electrostatic and ideal flow fields, the oscillation amplitudes of both the Ohmic current (ΔI) and flow rate (ΔQ) scale as [32–34]

$$\frac{\Delta Q}{\bar{Q}} \sim \frac{\Delta I}{\bar{I}} \sim \frac{V_p}{V_s} \sim \frac{d_p^3}{\bar{d}_j^3}, \tag{3}$$

where the sensing volume scales as $V_s \sim \bar{d}_j^3$, because the jet diameter is the only relevant scale at the apex (Fig. 1). Here, the overbar denotes the average (equilibrium) value and Δ denotes the peak amplitude of oscillation. When the volumetric flow (or Ohmic current) is dominated by axial convection (or axial conduction), $\Delta Q/\bar{Q}$ (or $\Delta I/\bar{I}$) scales as $\Delta d_j/\bar{d}_j$ for an approximately constant axial velocity (or electric field), as shown in Fig. 5.

Although not yet well understood, the phase shift between $\Delta d_j/\bar{d}_j$ (which presumably followed $\Delta Q/\bar{Q}$) and $\Delta I/\bar{I}$ appeared intrinsic to the complex electromechanical circuit. Similar phase shifts were observed between the sinusoidal driving voltage and the current response without any particle triggering, e.g., in the experiments described in Fig. 3.

B. Volume sensing

Among the possible indicators of the particle volume, the relative current change ($\Delta I/\bar{I}$) has a clear advantage for its ease of measurements. When the current oscillation had

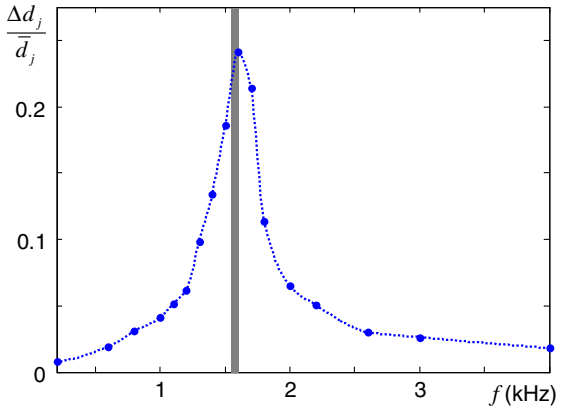

FIG. 4. The resonance of the cone-jet bridge. A sinusoidal voltage with a peak-to-peak amplitude of 20 V was added to the base voltage of 2.4 kV, and the relative change in the jet diameter ($\Delta d_j/\bar{d}_j$) was recorded at each driving frequency. Other conditions were the same as in Fig. 3. The frequency of the particle-triggered oscillation measured in the same system was 1576 $\pm$ 33 Hz (shaded area), coinciding with the measured resonant frequency of 1.6 kHz. The resonant and particle-triggered oscillations were shown at the top and bottom, respectively, of Video 2 [26].

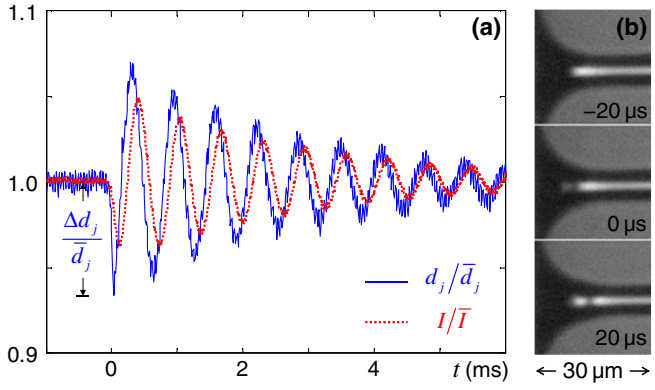

FIG. 5. Particle-triggered oscillations with conditions specified in Fig. 4. (a) Synchronized measurements of the diameter (d_j) and current (I) of the oscillating jet. Except for a phase shift, these oscillations were perfectly correlated. The impulse response up to the first maximum jet diameter was somewhat faster than subsequent oscillations; only periodic oscillations following the first maximum were used to measure the frequency. (b) The first minimum of jet diameter synchronized with a 7 μm particle entering the tip of the conical apex, within $\pm$20 μs. The synchronization is illustrated in Video 3 [30].

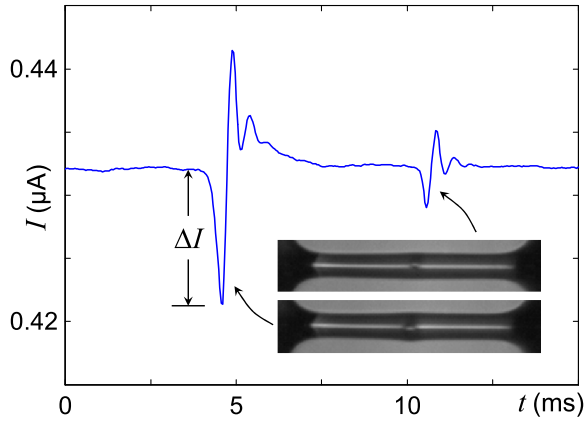

FIG. 6. Oscilloscopic and microscopic measurements confirming the resistive sensing of particles. A short nozzle length of 3 mm was chosen to provide a well-defined $\Delta I/\bar{I}$ with strong damping (cf. Fig. 5). When nonconducting particles with a diameter of 10 μm (bottom image) and 7 μm (top image) are passed through a cone-jet bridge with a diameter of 15 μm, the oscillations of the bridge current indicate the passage and relative size of these particles, which are confirmed with synchronized imaging in Video 4 [35].

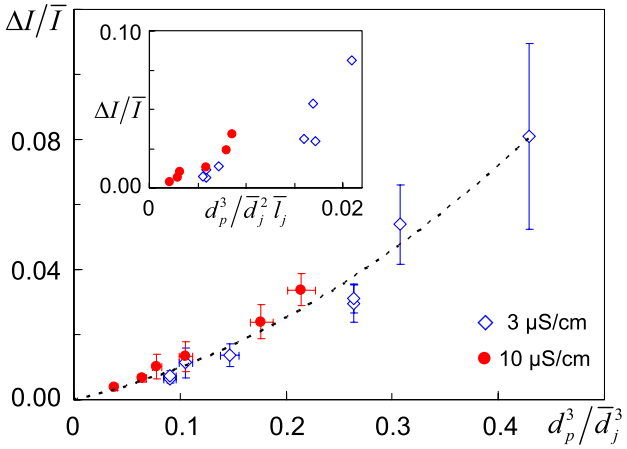

FIG. 7. Polystyrene particles were detected with the relative current change ($\Delta I/\bar{I}$) indicative of the ratio of the particle volume ($V_p \sim d_p^3$) to the sensing volume ($V_s \sim \bar{d}_j^3$). The vertical error bars are 95% confidence intervals of repeated measurements, while the horizontal ones are based on manufacturer specifications. For the dashed quadratic curve fit passing through the origin [Eq. (4)], $\alpha = 0.0719$, $\beta = 0.269$, and the coefficient of determination (R^2) is 0.963. In the inset, the relative current change correlates poorly with the particle-to-jet volume ratio, supporting the conclusion that the sensing volume is governed not by the volume of the jet ($\bar{d}_j^2 \bar{l}_j$) but by the volume of the conical apex ($\bar{d}_j^3$).

a rapid decay time, as in Fig. 6 where a short nozzle was used, $\Delta I/\bar{I}$ was a particularly robust indicator of the particle volume. For a dispersion of mixed particles, a larger depression of current (ΔI) indicated a larger particle, which was confirmed by synchronized imaging (Fig. 6 insets; see also Video 4 [35]).

Using the cone-jet bridge as the resistive Coulter sensor, micron-sized polystyrene particles were detected and sized (Fig. 7). Spherical particles with a diameter of 5 ± 0.1 μm (Duke Scientific 4205A beads), 7 ± 0.14 μm (4K-07) or 10 μm (G1000) were dispersed in ethylene glycol and doped to a conductivity (σ) of 3 or 10 μS/cm. Experimental conditions were similar to those described in Table I, with a voltage (V) of 1.35 or 1.45 kV at a fixed electrode separation (L) of 0.25 mm and a flow rate (Q) of 0.15 or 0.20 mL/h. Different combinations of σ, V, and Q were used to vary $\bar{d}_j$ while maintaining an approximately constant upstream conical shape. The high-frequency noise from the power source (apparent in Fig. 5) was electronically filtered.

Consistent with Eq. (3), all data in Fig. 7 collapsed as a function of $d_p^3/\bar{d}_j^3$,

$$\frac{\Delta I}{\bar{I}} \sim \alpha \frac{d_p^3}{\bar{d}_j^3} + \beta \frac{d_p^6}{\bar{d}_j^6} + \cdots, \tag{4}$$

where α and β are numerical constants. The second-order curve fit accounts for the effect of a finite particle size, similar to conventional Coulter counting [34]. From the curve fit in Fig. 7, the sensing region at the conical apex has an effective volume of $V_s \approx (2.4\bar{d}_j)^3$.

C. Discussions on cone-jet sensing apertures

Our resistive sensing technique based on the flexible cone-jet apertures is distinct from conventional Coulter counting with solid pores in three major aspects.

(i) Nonclogging sensing aperture.—The flexible sensing aperture defined by the air/liquid interface is immune to the clogging issue caused by impurities. In Fig. 8 (see also Video 5 [36]), which we reported in [10], a 30 μm-long piece of debris passed through a 14 μm-diameter jet without clogging, even when the longitudinal axis of the piece of debris turned from streamwise to spanwise with respect

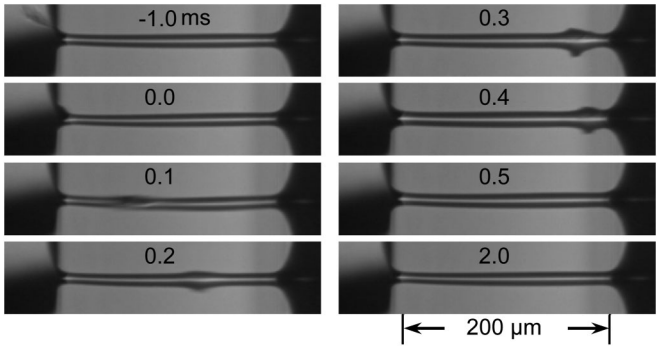

FIG. 8. The passage of a piece of debris twice the size of the equilibrium jet diameter. The bridging jet of 14 μm diameter self-adjusted to pass the 30 μm-long piece of debris, and relaxed back to its equilibrium configuration within 2 ms. The snapshots were captured from Video 5 [36].

to the jet. The cone-jet bridge quickly relaxed back to its equilibrium configuration (within 2 ms). Such a large piece of debris would have been detrimental to a solid pore with a diameter only half of its size.

As discussed in Sec. III A, the cone-jet bridge system was extremely robust, even against strong perturbations such as complete purging of the exposed working fluid. Therefore, the nonclogging aspect is fundamentally limited by the upstream nozzle diameter (d_n). We achieved Coulter counting with cone-jet bridges that issued from nozzles with a diameter as large as 1.6 mm.

(ii) Oscillatory current signature ($f \sim \sqrt{\gamma/\rho d_n^3}$).—The current signature is oscillatory at the resonant frequency (f) of the cone-jet bridge. The electromechanical oscillation sets a limit for the throughput of particle sensing, which can be improved with a smaller nozzle diameter (d_n), as indicated by Eq. (2). On the other hand, the resonance opens the possibility of resistive sensing with a ''lock-in'' frequency range.

With the 100 μm nozzles used here, a throughput of up to 1 kHz or so can be envisioned. Smaller nozzles can be used to increase the resonant frequency and therefore the throughput. However, there is a trade-off between high throughput and nonclogging Coulter counting because of their antagonistic dependence on the nozzle diameter.

(iii) Conical sensing volume ($V_s \sim \bar{d}_j^3$).—The sensing region scales as the volume of the conical apex ($\bar{d}_j^3$), which is only a function of the jet diameter, as indicated by Eq. (3). Had the jet been replaced by a fixed solid pore with the same dimensions, the sensing volume would be the volume of the jet ($\bar{d}_j^2 \bar{l}_j$), which is also a function of the jet length ($\bar{l}_j$). See Fig. 7 for a comparison of these two scalings. This subtle difference was not easy to discern with long nozzles, which yielded much smaller (and more scattered) $\Delta I/\bar{I}$, as discussed in [10].

The new $\bar{d}_j^3$ scaling of the sensing volume is favorable for improving the analysis range by reducing the jet diameter. With the conditions represented by Table I, the cone-jet bridge had a diameter typically above 10 μm. Although we did not systematically investigate the lower bound, smaller bridge diameter could be obtained; e.g., a 5 μm-diameter bridge was produced using a smaller nozzle with an outer diameter of 30 μm. Using the cone-jet liquid bridge, we reliably detected particles as small as 30% of the cone-jet aperture diameter ($\bar{d}_j$). With more specialized electronics instead of a generic oscilloscope for current measurements, even smaller particles should be detectable.

V. CONCLUDING REMARKS

In summary, we produced a cone-jet bridge carrying primarily Ohmic current and used it for resistive (volumetric) sensing of particles. Triggered by a particle passing through the conical apex, the relative current change is indicative of the particle-to-jet diameter ratio (not the volume ratio). A main advantage of the jet-based Coulter counting is its immunity to clogging by impurities and agglomerates, thanks to the flexible air/liquid interface defining the sensing aperture.

For the mechanistic study here, we have reported only Coulter counting with the cone-jet bridge, where the analysis range was limited by the relatively large jet diameter. However, we have also demonstrated Coulter counting with the conventional Taylor cone-jet, where the jet diameter can in principle be tuned down to 10 nm (by using a high-conductivity fluid [5]). Compared to Coulter counting with the cone-jet bridge reported above, our preliminary results indicated that Coulter counting with the Taylor cone-jet shares many common characteristics. For example, both cases have a nonclogging sensing aperture with an oscillatory current signature around the Rayleigh oscillation frequency, Eq. (2). On the other hand, the two techniques have complementary analysis ranges, with the cone-jet bridge more suitable for micrometric particles (such as biological cells) while the conventional Taylor cone-jet is more suitable for nanometric particles (such as viruses). Combined with the drop-and-place technique [37,38], electrohydrodynamic Coulter counting has the potential to enable the sensing and deployment of a broad range of particles.

ACKNOWLEDGMENTS

This work was supported by the National Science Foundation Grant No. CBET-08-46705. We thank J. Kim, F. Liu, and W. Scheideler for helpful discussions.

[1] W. Coulter, Means for Counting a Particle Suspended in a Fluid, U.S. Patent No. 2,656,508 (1953).
[2] http://www.beckmancoulter.com.
[3] G. Taylor, *Disintegration of Water Drops in an Electric Field*, Proc. R. Soc. A **280**, 383 (1964).
[4] M. Cloupeau and B. Prunet-Foch, *Electrostatic Spraying of Liquids in Cone-Jet Mode*, J. Electrost. **22**, 135 (1989).
[5] J. Fernandez de la Mora, *The Fluid Dynamics of Taylor Cones*, Annu. Rev. Fluid Mech. **39**, 217 (2007).
[6] H. Gonzalez, M. McCluskey, A. Castellanos, and A. Barrero, *Stabilization of Dielectric Liquid Bridges by Electric Fields in the Absence of Gravity*, J. Fluid Mech. **206**, 545 (1989).
[7] A. Klingner, S. Herminghaus, and F. Mugele, *Self-Excited Oscillatory Dynamics of Capillary Bridges in Electric Fields*, Appl. Phys. Lett. **82**, 4187 (2003).
[8] E. Fuchs, J. Woisetschlager, K. Gatterer, E. Maier, R. Pecnik, G. Holler, and H. Eisenkolbl, *The Floating Water Bridge*, J. Phys. D **40**, 6112 (2007).
[9] J. Bird, W. Ristenpart, A. Belmonte, and H. Stone, *Critical Angle for Electrically Driven Coalescence of Two Conical Droplets*, Phys. Rev. Lett. **103**, 164502 (2009).

[10] Y. Zhao and C. Chen, in Proceedings of the 14th International Conference on Miniaturized Systems for Chemistry and Life Sciences (μTAS), Groningen, Netherlands, 2010, pp. 620–622. Note that nozzles of approximately 20 mm length were used in this paper.

[11] Y. Zhao, J. Boreyko, M. Chiang, C. Baker, and C. Chen, in Proceedings of the 2nd International Conference on Micro/Nanoscale Heat and Mass Transfer, Shanghai, 2009, Vol. 3, pp. 439–441.

[12] D. Saville, *Electrohydrodynamics: The Taylor-Melcher Leaky Dielectric Model*, Annu. Rev. Fluid Mech. **29**, 27 (1997).

[13] See Supplemental Material at http://link.aps.org/supplemental/10.1103/PhysRevX.1.021007 for Video 1: Formation process of a cone-jet bridge (Fig.2). This video was captured at 20 000 fps and played back at 100 fps, with a field of view of 0.25 mm $\times$ 0.17 mm.

[14] *Handbook of Chemistry and Physics*, edited by W. Haynes (CRC Press, Boca Raton, 2011), 91st ed.

[15] I. Marginean, P. Nemes, L. Parvin, and A. Vertes, *How Much Charge Is There on a Pulsating Taylor Cone?* Appl. Phys. Lett. **89**, 064104 (2006).

[16] R. Sabate, L. Freire, and J. Estelrich, *Influence of Dielectric Constant on the Spectral Behavior of Pinacyanol*, J. Chem. Educ. **78**, 243 (2001).

[17] J. Fernandez de la Mora and I. Loscertales, *The Current Emitted by Highly Conducting Taylor Cones*, J. Fluid Mech. **260**, 155 (1994).

[18] A. Ganan-Calvo, J. Davila, and A. Barrero, *Current and Droplet Size in the Electrospraying of Liquids. Scaling Laws*, J. Aerosol Sci. **28**, 249 (1997).

[19] C. Chen, in *Electrokinetics and Electrohydrodynamics in Microsystems*, edited by A. Ramos (Springer, New York, 2011), pp. 177–220 [http://www.springer.com/engineering/book/978-3-7091-0899-4].

[20] M. Hohman, M. Shin, G. Rutledge, and M. Brenner, *Electrospinning and Electrically Forced Jets. I. Stability Theory*, Phys. Fluids **13**, 2201 (2001).

[21] J. Melcher and E. Warren, *Electrohydrodynamics of a Current-Carrying Semi-insulating Jet*, J. Fluid Mech. **47**, 127 (1971).

[22] C. Burcham and D. Saville, *The Electrohydrodynamic Stability of a Liquid Bridge: Microgravity Experiments on a Bridge Suspended in a Dielectric Gas*, J. Fluid Mech. **405**, 37 (2000).

[23] C. Burcham and D. Saville, *Electrohydrodynamic Stability: Taylor-Melcher Theory for a Liquid Bridge Suspended in a Dielectric Gas*, J. Fluid Mech. **452**, 163 (2002).

[24] A. Widom, J. Swain, J. Silverberg, S. Sivasubramanian, and Y. Srivastava, *Theory of the Maxwell Pressure Tensor and the Tension in a Water Bridge*, Phys. Rev. E **80**, 016301 (2009).

[25] A. Marin and D. Lohse, *Building Water Bridges in Air: Electrohydrodynamics of the Floating Water Bridge*, Phys. Fluids **22**, 122104 (2010).

[26] See Supplemental Material at http://link.aps.org/supplemental/10.1103/PhysRevX.1.021007 for Video 2: Resonant vs particle-triggered oscillation (Figs. 3 and 4). The particle diameter was 7 μm. This video was captured at 30 000 fps and played back at 15 fps, with a field of view of 0.17 mm $\times$ 0.07 mm.

[27] Lord Rayleigh, *On the Equilibrium of Liquid Conducting Masses Charged with Electricity*, Philos. Mag. **14**, 184 (1882).

[28] D. Bober and C. Chen, *Pulsating Electrohydrodynamic Cone-Jets: From Choked Jet to Oscillating Cone*, J. Fluid Mech. (to be published).

[29] A. Ganan-Calvo, *On the Theory of Electrohydrodynamically Driven Capillary Jets*, J. Fluid Mech. **335**, 165 (1997).

[30] See Supplemental Material at http://link.aps.org/supplemental/10.1103/PhysRevX.1.021007 for Video 3: Jet diameter vs particle position (Fig. 5). The particle diameter was 7 μm. This video was captured at 100 000 fps and played back at 25 fps, with a field of view of 0.17 mm $\times$ 0.03 mm.

[31] A. Barrero, A. Ganan-Calvo, J. Davila, A. Palacio, and E. Gomez-Gonzalez, *Low and High Reynolds Number Flows inside Taylor Cones*, Phys. Rev. E **58**, 7309 (1998).

[32] J. Maxwell, *A Treatise on Electricity and Magnetism* (Clarendon Press, Oxford, 1891), 3rd ed., Vol. I, p. 440; *A Treatise on Electricity and Magnetism* (Dover, Mineola, 1954).

[33] W. Smythe, *Flow around a Sphere in a Circular Tube*, Phys. Fluids **4**, 756 (1961).

[34] R. DeBlois and C. Bean, *Counting and Sizing of Submicron Particles by the Resistive Pulse Technique*, Rev. Sci. Instrum. **41**, 909 (1970).

[35] See Supplemental Material at http://link.aps.org/supplemental/10.1103/PhysRevX.1.021007 for Video 4: Microscopic confirmation of resistive sensing of particles with a diameter of 10 μm and 7 μm, respectively (Fig. 6). This video starts at 0 ms and ends at 15 ms, corresponding to the current oscillogram in Fig. 6. This video was captured at 68 000 fps and played back at 50 fps, with a field of view of 0.18 mm $\times$ 0.04 mm.

[36] See Supplemental Material at http://link.aps.org/supplemental/10.1103/PhysRevX.1.021007 for Video 5: Passage of a large piece of debris without clogging (Fig. 8). This video was captured at 40 000 fps and played back at 20 fps, with a field of view of 0.31 mm $\times$ 0.07 mm.

[37] C. Chen, D. Saville, and I. Aksay, *Electrohydrodynamic "Drop-and-Place" Particle Deployment*, Appl. Phys. Lett. **88**, 154104 (2006).

[38] C. Chen, D. Saville, and I. Aksay, *Scaling Laws for Pulsed Electrohydrodynamic Drop Formation*, Appl. Phys. Lett. **89**, 124103 (2006).